Research article

Journal of MASS SPECTROMETRY

Received: 4 December 2013 Revised: 18 April 2014 Accepted: 24 April 2014 Published online in Wiley Online Library

(wileyonlinelibrary.com) DOI 10.1002/jms.3384

New MALDI matrices based on lithium salts for the analysis of hydrocarbons and wax esters

Petra Horká,[a,b] Vladimír Vrkoslav,[b] Robert Hanus,[b] Karolina Pecková[a] and Josef Cvačka[b]*

Lithium salts of organic aromatic acids (lithium benzoate, lithium salicylate, lithium vanillate, lithium 2,5-dimethoxybenzoate, lithium 2,5-dihydroxyterephthalate, lithium α-cyano-4-hydroxycinnamate and lithium sinapate) were synthesized and tested as potential matrices for the matrix-assisted laser desorption/ionization (MALDI)-mass spectrometry analysis of hydrocarbons and wax esters. The analytes were desorbed using nitrogen laser (337.1 nm) and ionized via the attachment of a lithium cation, yielding $[M+Li]^+$ adducts. The sample preparation and the experimental conditions were optimized for each matrix using stearyl behenate and *n*-triacontane standards. The performance of the new matrices in terms of signal intensity and reproducibility, the mass range occupied by matrix ions and the laser power threshold were studied and compared with a previously recommended lithium 2,5-dihydroxybenzoate matrix (LiDHB) (Cvačka and Svatoš, *Rapid Commun. Mass Spectrom.* 2003, *17*, 2203). Several of the new matrices performed better than LiDHB. Lithium vanillate offered a 2–3 times and 7–9 times higher signal for wax esters and hydrocarbons, respectively. Also, the signal reproducibility improved substantially, making this matrix a suitable candidate for imaging applications. In addition, the diffuse reflectance spectra and solubility of the synthesized compounds were investigated and discussed with respect to the compound's ability to serve as MALDI matrices. The applicability of selected matrices was tested on natural samples of wax esters and hydrocarbons. Copyright © 2014 John Wiley & Sons, Ltd.

Additional supporting information may be found in the online version of this article at the publisher's web-site.

Keywords: cuticular hydrocarbons; lipids; lithium attachment; MALDI matrix; waxes

Introduction

Long-chain hydrocarbons (HCs) and long-chain oxygen-containing lipids including wax esters (WEs) are vital molecules in all forms of life.[1–5] A variety of approaches based on mass spectrometry (MS) are used to detect, quantify and characterize these compounds. Gas chromatography (GC) is usually considered for sufficiently volatile lipids. For long-chain species, high-temperature columns are preferably used,[6–8] and informative EI spectra with abundant molecular ions can be obtained using supersonic molecular beam technology.[9,10] Liquid chromatography does not require a high volatility of the analytes and offers efficient separations of long-chain neutral lipid species, usually in reversed-phase or silver-ion systems.[11–16] Several ionization methods including atmospheric-pressure chemical ionization[12,17–19] or electrospray[20–23] have been shown to be useful for MS detection of these compounds.

The use of chromatographic separations prior to MS is essential for a comprehensive characterization of complex samples. However, direct MS is a powerful alternative for samples of low complexity or for high-throughput screening approaches. Desorption/ionization MS techniques are very useful in this respect, including nowadays seldom used field desorption,[24,25] desorption electrospray,[26,27] desorption atmospheric pressure photoionization,[28] laser desorption/ionization[29–32] and matrix-assisted laser desorption/ionization (MALDI).[33–38] Desorption/ionization MS techniques are also indispensable for MS imaging (MSI).[39–42] As regards MALDI and long-chain neutral lipids, addition of silver salts to the sample yields $[M+Ag]^+$ ions.[29,30,43–47] This approach offers appreciable sensitivity, but the data interpretation is complicated because of the occurrence of two almost equally abundant silver isotopes. Moreover, dehydrogenation of analytes[45] and persistent contamination of MALDI targets[48] have also been reported. An alternative approach is based on cationization with lithium ions,[34] which yields $[M+Li]^+$ adducts. Naturally occurring lithium is composed mostly of ^7Li (92.5%), which results in less complex isotope profiles and thus significantly simplifies data interpretation. In addition, both ^7Li and ^6Li are commercially available and affordable, which offers the ultimate simplification of the isotope profiles. In our previous work, lithium 2,5-dihydroxybenzoate (LiDHB) was suggested as an appropriate MALDI matrix for several neutral lipid classes including HCs and WEs,[34,36,37] and the use of the matrix for MSI of cuticular lipids was demonstrated as well.[39] Although the sensitivity of MALDI-MS with LiDHB is fairly good, the efficiency of the lithium cationization might further be enhanced using new matrices with a modified chemical structure. The matrix properties can be tuned by changing substituents on the benzene ring, allowing for an alteration of absorption

* *Correspondence to: Josef Cvačka, Institute of Organic Chemistry and Biochemistry, v.v.i., Academy of Sciences of the Czech Republic, Flemingovo nám. 2, CZ-166 10 Prague 6, Czech Republic. E-mail: cvacka@uochb.cas.cz*

a *Department of Analytical Chemistry, University Centre of Excellence 'Supramolecular Chemistry', Faculty of Science, Charles University in Prague, Hlavova 2030/8, CZ-128 43 Prague 2, Czech Republic*

b *Institute of Organic Chemistry and Biochemistry, v.v.i., Academy of Sciences of the Czech Republic, Flemingovo nám. 2, CZ-166 10 Prague 6, Czech Republic*

Journal of MASS SPECTROMETRY

coefficients at a given laser wavelength and an improvement of physico-chemical properties affecting co-crystallization with the analyte, and thus homogeneity of the sample deposits. The formation of $[M+Li]^+$ in the gas phase can proceed via direct attachment of free lithium cation, and/or by lithium ion transfer from the cationized matrix.[49] As lithium cation can form various chelate complexes with the substituents on the benzene ring,[50] the substituents also change gas-phase lithium cation basicity of the matrix (negative of the Gibbs free energy associated with the reaction $B_{(g)} + Li^+_{(g)} \rightarrow B\text{-}Li^+_{(g)}$) and thus its ability to transfer lithium cation to the analyte.

In this work, we synthesized and tested several lithium salts of aromatic carboxylic acids as potential MALDI matrices for lithium cationization of HCs and WEs. The matrices were characterized by elemental analysis, diffuse reflectance spectroscopy, MS and solubility measurements. Their performance as MALDI matrices was thoroughly tested and compared with the LiDHB matrix.

Materials and methods

Reagents and chemicals

Benzoic acid, salicylic acid, vanillic acid, 2,5-dimethoxybenzoic acid, 2,5-dihydroxyterephthalic acid, α-cyano-4-hydroxycinnamic acid (HCCA), sinapic acid, 2,5-dihydroxybenzoic acid (DHB) and Li_2CO_3 of the highest available purity were purchased from Sigma-Aldrich (St. Louis, MO, USA).

The methanol for HPLC (Sigma-Aldrich, St. Louis, MO, USA) was used as received; the other solvents (chloroform, diethyl ether and hexane) were distilled in glass from analytical-grade solvents. Rhodamine 6G (purity 99%), $MgSO_4$ (purity 99.5%), $BaSO_4$ (purity 99%) and polyethylene glycols (PEGs 200, 400, 600, 1000) were purchased from Sigma-Aldrich. The aqueous calibration solution of lithium (1000 ppm) was purchased from ANALYTIKA (Prague, Czech Republic) and silica gel 60G from Merck (Darmstadt, Germany).

Matrix synthesis

The matrices were synthesized by neutralizing the acids with Li_2CO_3 as described previously.[37] Briefly, acids (0.2–5.2 g) were dissolved in deionized water (15–50 ml; Milli-Q, Millipore) at room or higher temperature, depending on their solubility, and a stoichiometric amount of Li_2CO_3 was slowly added. The pH of the reaction mixtures was kept in a weakly acidic range to avoid oxidation of the compounds to colored products, likely quinones,[51] by molecular oxygen. The products were crystallized after the reaction mixture was cooled to 4 °C in a refrigerator. The crystals were obtained by filtration and dried to constant weight in a desiccator (ca. 48 h. at room temperature) to remove residual moisture. The reaction conditions are specified in the supporting information, Table S2.

Lipid samples

The standards of stearyl behenate and *n*-triacontane (Sigma-Aldrich, purity 99%) were dissolved in $CHCl_3$ (0.25 mg/ml and 0.02 mg/ml, respectively). The mixtures of WEs and HCs were isolated from various sources using semipreparative TLC. *Ginkgo biloba* leaves (12 pieces) were washed three times with 25 ml of $CHCl_3$; virgin beeswax (116 mg) was dissolved in 2 ml of $CHCl_3$ and cuticular lipids of grey flesh fly *Neobellieria bullata* were extracted as described previously.[37] Parafilm® M laboratory sealing film (6.0 g, Pechiney Plastic Packaging Company, Chicago, IL, USA) was extracted with $CHCl_3$ (40 ml) at 50 °C. The lipid extracts were filtered using purified cotton wool, dried with anhydrous $MgSO_4$, and the solvent was evaporated under a stream of nitrogen. The residues were reconstituted in hexane and separated on pre-cleaned glass TLC plates (59 × 76 mm) coated with silica gel 60G with gypsum (12%). The mobile phase was either hexane:diethyl ether (93:7, *v/v*; for WEs) or hexane (for HCs). The TLC zones were visualized by spraying with rhodamine 6G solution (0.05% in ethanol) and inspected under UV light (254 nm). The zones corresponding to HCs and WEs were scraped off the plates and extracted with 10 ml of freshly distilled diethyl ether. After evaporation of the solvent, the lipid mixtures were dissolved in $CHCl_3$ (10 mg/ml).

Elemental analysis

The classical elemental analysis performed on a PE 2400 Series II CHNS/O Analyzer (Perkin Elmer, Waltham, MA, USA) was used to determine the amount of crystallization water in the newly synthesized matrices. The degree of hydration of the crystals was established by comparing the experimental content of carbon, hydrogen and nitrogen with the theoretical values calculated for possible hydrates.

Atomic emission spectroscopy

The amount of lithium in the matrices was determined by atomic emission spectroscopy (AES). The analyses were performed on flame spectrometer AAS 3 (Carl Zeiss Jena, Germany) set to monitor lithium emission at 670.7 nm. The concentrations were calculated from calibration curves (0–3.0 ppm) obtained by measuring standard solutions of lithium and solutions of matrices prepared in water for a theoretical lithium concentration of 1 ppm.

Diffuse reflection spectroscopy of solid matrices

A single-beam LAMBDA 35 UV/Vis spectrometer (PerkinElmer, USA) equipped with RSA-PE-20 integrating sphere (Labsphere, USA) was used for the measurement of the diffuse reflectance spectra of solid samples. The matrices (100 mg) were carefully grinded with $BaSO_4$ (Merck, for white standard DIN 5033; 900 mg) in an agate mortar. The spectra (reflectance in % values *vs* wavelength) were taken in quartz cells in the 250–600 nm range with the slit width 2 nm. $BaSO_4$ served as the reflectance calibration standard (100% reflectance). The diffuse reflectance spectra were transformed using the Kubelka–Munk function ($F(R) = (1-R)^2/2R$, where R is reflectance, i.e. fraction of incident radiation reflected by a surface; $0 \le R \le 1$) to obtain an approximation of absorption spectra.[52] The spectra were averaged from 12 measurements.

Ultraviolet–visible spectroscopy of matrices in solution

The ultraviolet and visible spectra of the matrices prepared in water at a concentration of 5×10^{-5} mol/l were acquired using the Hewlett-Packard 8453 single-beam spectrophotometer with collimating optics. The absorption spectra were recorded from 200 to 600 nm using a path length of 10 mm and a bandwidth of 1.0 nm.

MALDI-MS

MALDI-TOF experiments were performed on Reflex IV (Bruker Daltonics, Bremen, Germany) operated in reflectron mode with an acceleration voltage of 20 kV and an extraction pulse duration of 200 ns. Desorption and ionization were achieved using a MNL 100 pulsed nitrogen laser (337.1 nm; pulse halfwidth 3 ns, pulse energy ≥155 μJ; LTB Lasertechnik Berlin, Germany). The laser repetition rate was set to 9 Hz, and the laser fluence was adjusted in 0–100% range by a circular variable attenuator. The laser pulse energy measured in the Scout MTP ion source close to the focal plane exhibited exponential dependence on the laser attenuator setting (see supporting information for details). The PEM100 energy meter (LTB Lasertechnik Berlin) was used for laser pulse energy measurements. The laser energy stability was ≤2% according to the manufacturer's specifications. The focal spot size was estimated from the dimensions of ablated area on the thin layer of α-HCCA (Bruker's pre-spotted stainless steel target); laser attenuated to 50% (1.1 μJ) burned elliptical spot 33 μm × 131 μm. With the exception of matrix-ion studies, deflection was used to suppress matrix ions up to *m/z* 210. Data were collected and analyzed using FlexAnalysis 3.0 software (Bruker Daltonics). The samples and matrices (1.5 μl) were deposited on the MALDI MTP 384-position ground steel target (Bruker Daltonics), precleaned by washing with ethanol and $CHCl_3$/CH_3OH (1:2, *v/v*) followed by a sonication in $CHCl_3$ and air-dried. The matrices were dissolved in $CHCl_3$/CH_3OH (3:1, *v/v*) at a concentration of 10.0 mg/ml (all matrices with the exception of Li_2DHT) or $CHCl_3$/CH_3OH (1:4, *v/v*) at a concentration of 0.75 mg/ml (Li_2DHT); the standards were dissolved in $CHCl_3$. The mass spectra were externally calibrated using a mixture of PEGs (200, 400, 600 and 1000).

Statistics

In order to evaluate the reproducibility of MALDI measurements using particular matrices with complex samples, we used principal component analysis (PCA) on the data resulting from the analysis of cuticular HCs extracted from the body surface of *N. bullata*. The relative intensities corresponding to $[M + Li]^+$ adducts of the sample measured repeatedly using LiVA, LiDHB and LiSA matrices were used for the PCA, and the factor scores of the first two factors (components) were visualized in a scatter plot in Statistica 8 (StatSoft, Tulsa, USA).

Results and discussion

The structure and physico-chemical properties of the matrices

The newly synthesized matrices (Table 1) were crystallized from water solutions, which could eventuate in the formation of hydrates. To determine the number of the moles of crystallization water possibly present in the crystals, a classical C, H and N elemental analysis of the solid samples was used. The results indicated that the matrices were indeed hydrous substances with up to 2.5 moles of water per mole of matrix (LiDHB was previously shown to crystallize from water solution as tetrahydrate[36]). The chemical composition of the matrices was further verified by measuring lithium content using AES. The theoretical and measured percent composition of the matrices is given in the supporting information (Table S3).

The ability of matrices to form homogenous sample deposits is a crucial factor underlying their practical usefulness. As the sample deposits were formed from a liquid phase (matrix and sample solutions), matrix solubilities in various solvents were investigated. As expected, the matrices were well soluble in polar solvents such as water, methanol and ethanol. More importantly, some of the newly synthesized matrices were appreciably soluble also in hexane (LiSalA, LiVA), diethyl ether (LiBA, LiSA), chloroform (LiVA) or acetone (LiSalA, LiDHB, LiVA). The solubility data are included in the supporting information (Table S4).

MALDI matrices should efficiently absorb the energy of the laser. Therefore, matrix optical properties affect their ability to facilitate the MALDI process. The matrices with aromatic rings are usually used in UV MALDI, as they have sufficiently high molar absorption coefficients in a certain wavelength range. In this work, ultraviolet absorptions of the benzene ring were modified by several substituents, namely hydroxy, methoxy, carboxy, 2-carboxyethenyl and 2-carboxy(2-cyanoethyl)ethenyl groups (carboxyls were in the form of lithium salts). In order to characterize the abilities of the matrices to absorb laser radiation, their UV/VIS spectra were recorded both in solution and solid state (Fig. 1). Solid-state absorption spectra were obtained by diffuse reflection spectroscopy of the matrix crystals carefully grinded with $BaSO_4$. Kubelka–Munk transformation[53] was subsequently applied to obtain peak patterns analogous to transmission absorbance spectra.[52] When compared to solution spectra, the solid-state spectral absorption bands tended to be broadened, and their maxima shifted toward longer wavelengths. The solid-state spectra were not recorded for LiSalA and LiDHB because of strong emission of fluorescence light, which the instrument could not filter out. Solid-state UV absorption peak of DHB is known from literature[54] to be broader and significantly red-shifted than in the solution, which likely applies also for LiDHB. The benzene-ring substitution had a significant effect on the UV/VIS spectra of the matrices and the magnitude of absorption coefficients at the nitrogen laser wavelength (Table 1). LiHCCA showed exceptionally high absorption at 337 nm and Li_2DHT also significantly absorbed UV light at nitrogen laser wavelength. For most of other matrices, the laser wavelength appeared at the descending part of the absorption peak measured in the solution, often close to the peak end (LiSalA, LiDMB, LiSA), sometimes even outside the peak (LiBA, LiVA). As the absorption bands in solid state spectra were broader and shifted toward longer wavelengths, all matrices absorbed radiation at 337 nm in solid state with the exception of LiBA, which did not absorb radiation above 300 nm at all.

Matrix cluster ions

After irradiating by a laser pulse, the matrices produced complex mixtures of ions. The nature of these ions and the mass ranges occupied by them were briefly characterized. The matrices commonly formed singly charged protonated molecules $[matrix + H]^+$ and adducts with lithium $[matrix + Li]^+$, which also eliminated CO_2 and/or H_2O; a neutral loss of HCN was observed in the case of LiHCCA. Lithium/hydrogen exchanges were also common, yielding $[matrix\text{-}H + 2Li]^+$. The formation of dimeric or trimeric ions ($[2matrix + Li]^+$, $[3matrix + Li]^+$) was noticed at higher laser fluences. In the very low mass region, lithium cation along with impurities of other alkali metal ions (Na^+, K^+) occurred. The high laser pulse energies (3.2 μJ) induced the generation of Cr^+ from the stainless-steel plate[37] (LiDMB, LiBA). The mass spectra of the matrices are included in the supporting information (Figs.

Journal of MASS SPECTROMETRY

Table 1. An overview of the matrices investigated

Matrix		Water of crystallization (mole) [a]	Absorption/reflectance at 337 nm	
			In solution (10^3 A.U.)	In solid state (10^3 K-M units)
Lithium benzoate LiBA	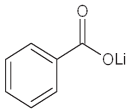	0	<1.0	<1.0
Lithium salicylate LiSalA	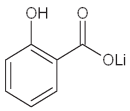	1	2.3	– [b]
Lithium vanillate LiVA	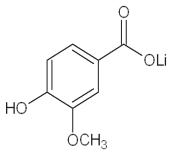	2	<1.0	25.7
Lithium 2,5-dimethoxybenzoate LiDMB	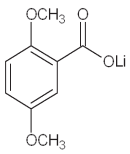	1	2.5	52.9
Lithium 2,5-dihydroxyterephthalate Li_2DHT	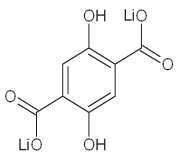	0.25	244.3	418.7
Lithium α-cyano-4-hydroxycinnamate LiHCCA	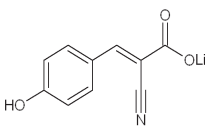	1	1182.9	561.0
Lithium sinapate LiSA	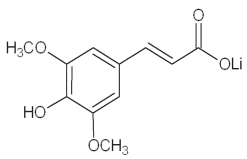	2.5	282.2	450.2
Lithium 2,5-dihydroxybenzoate LiDHB	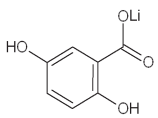	4 [c]	142.1	– [b]

[a]The number of the moles of crystallization water per mole of compound.
[b]The reflectance spectra were not obtained because of the matrix fluorescence.
[c]From Ref. [36]

S2–S9). From the practical point of view, the *m/z* range of the spectrum occupied by matrix ions is an important criterion for matrix selection. The highest *m/z* values of matrix ions generated at the optimum laser pulse energy (Table 2) ranged virtually from zero (LiVA) up to ~*m/z* 590 (LiDMB); see Fig. 2. High-mass matrix-ion clusters were found in matrices requiring a high laser setting

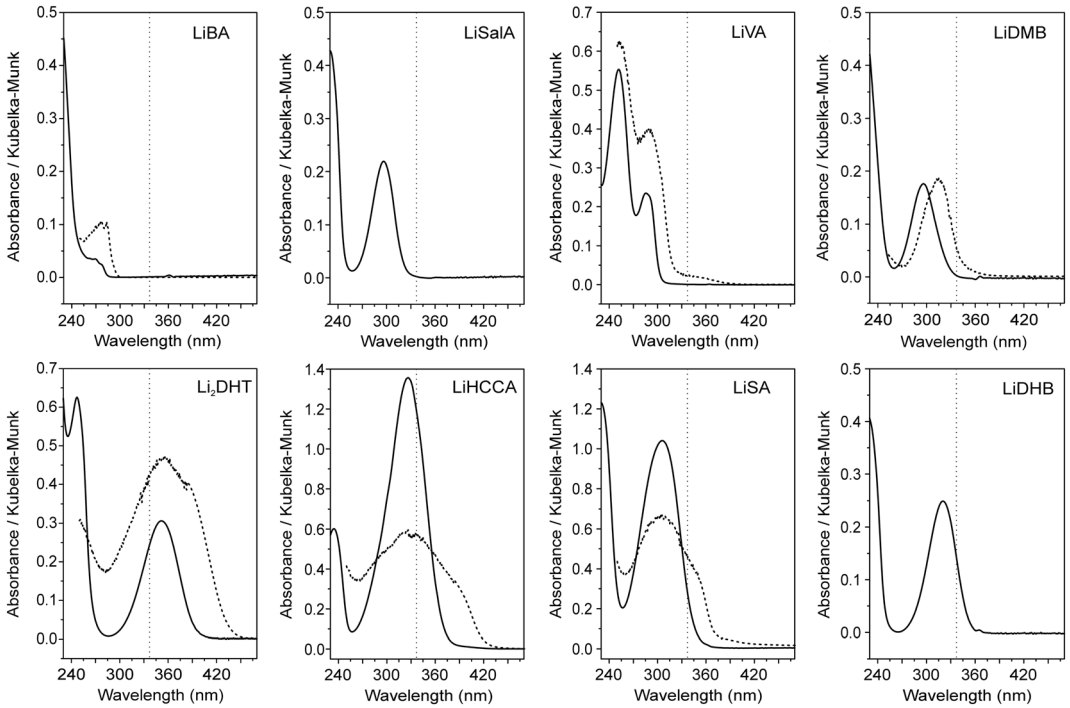

Figure 1. The UV/VIS spectra of the matrices dissolved in water (solid line) and Kubelka–Munk function-transformed diffuse reflectance spectra of powdered matrices diluted with $BaSO_4$ (dotted line).

Table 2. Sample preparation methods and laser settings for the matrices investigated and standard compounds

Matrix	Sample preparation		Laser pulse energy (μJ)[a]	
	WE	HC	WE	HC
LiBA	TL	DD	1.9/**3.2**	–/–[b]
LiSalA	TL	TL	0.6/**1.1**	0.9/**1.6**
LiVA	DD	DD	0.3/**0.6**	0.3/**0.6**
LiDMB	TL	RTL	0.5/**0.8**	–/–[b]
Li_2DHT	DD	DD	0.4/**0.8**	0.6/**1.1**
LiHCCA	RTL	DD	0.4/**0.7**	0.5/**0.9**
LiSA	TL	DD	0.4/**0.7**	0.4/**0.8**
LiDHB	TL	TL	0.5/**0.8**	0.3/**0.9**

[a]The minimum/**optimum** value; an average of three to five measurements.
[b]No signal at any laser fluence.

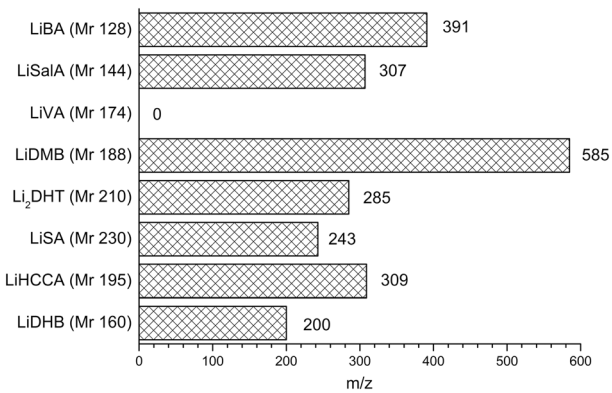

Figure 2. The *m/z* ranges occupied by the matrix ions at the optimum laser pulse energy for *n*-triacontane (the upper *m/z* limits for stearyl behenate laser settings were the same or lower). LiVA did not provide matrix ions at its optimum laser settings; data shown for slightly elevated laser pulse energy. LiDHB data were taken from Ref. [37].

for the ionization of analytes (LiDMB, LiBA). The best matrix with respect to matrix ions was LiVA, which required the lowest laser pulse energy (0.6 μJ). At this laser fluence, no matrix ions were detected (Fig. S4). A slightly higher laser setting (0.7 μJ) yielded matrix ions ranging up to ~*m/z* 190 (Fig. S5).

Optimization of sample preparation protocols

A sample preparation protocol was thoroughly optimized for each matrix. Three procedures were compared: the thin-layer method (TL; matrix first, sample after solvent evaporation), the reversed thin-layer method (RTL; sample first, matrix after solvent evaporation) and the dried-droplet method (DD; deposition of an admixture of the sample and matrix prepared in a 100-μl vial insert). For these experiments, stearyl behenate or *n*-triacontane (prepared in $CHCl_3$, 10 mg/ml, 1.5 μl) was co-deposited as the analyte with a matrix solution ($CHCl_3/CH_3OH$, 1.5 μl).

First, the minimum and optimum energy of the laser beam pulse was determined for each sample (the minimum pulse energy: the lowest laser setting at which the analyte signal appears; the optimum pulse energy: the laser setting at which the signal intensity is sufficiently high, peaks remain narrow and noise-level is still low). Above the optimum laser fluence, the signal continued to grow, but the resolution slowly deteriorated because of peak broadening and matrix ions started to appear also at higher *m/z* values. The minimum and optimum laser

pulse energy values were found to be almost independent of the sample preparation protocol. The optimum laser pulse energies were comparable for almost all matrices (0.7–1.1 μJ for stearyl behenate, 0.8–1.6 μJ for *n*-triacontane), with the exception of LiBA and LiDMB. LiBA required a much higher laser setting for stearyl behenate and failed to provide detectable lithium adducts of *n*-triacontane, similarly to LiDMB (Table 2). The laser fluences needed for generation of lithium adducts from stearyl behenate and *n*-triacontane were roughly 2–3 higher than those required for peptides in the α-HCCA matrix. Peptides of the Bruker's calibration peptide mixture deposited by the dried droplet method provided optimum signals at laser pulse energy ca. 0.4 μJ.

The optimum sample preparation protocol was sought for each matrix. The protocols were evaluated based on the intensity of the $[M + Li]^+$ peaks (18 spectra averaged, 600 shots). In general, the highest signals of *n*-triacontane were mostly obtained with DD, whereas stearyl behenate was usually better detected from samples prepared using TL (Table 2). The appropriate matrix-to-analyte ratios were determined from signal intensities, when matrix solutions (10.0 mg/ml in $CHCl_3/CH_3OH$; 0.75 mg/ml for Li_2DHT) were co-deposited with the standards (0.01–1.40 mg/ml for stearyl behenate, 0.1–1.3 mg/ml for *n*-triacontane). The highest signals were observed at a matrix-to-analyte molar ratio of 100:1 (stearyl behenate) and 10:1 (*n*-triacontane). The only exception was Li_2DHT, working the best at 10:1 (stearyl behenate) and 2:1 (*n*-triacontane). These ratios were consistent with our previous results with LiDHB[37] and similar to those of other lipids and low-molecular compounds, usually requiring a smaller surplus of the matrix than, e.g. proteins or peptides.[55–58]

The performance of the matrices under optimized conditions

The matrices were compared under optimized conditions (sample-preparation protocol, matrix-to-analyte ratio and optimum laser power) using stearyl behenate and *n*-triacontane standards. The samples were deposited in triplicates at random positions on the MTP plate and unbiased data were recorded using an automatic measurement mode. The spectra were collected 10 times for each sample position and averaged from 1000 shots (spectra from the first 20 shots were discarded). Altogether, 30 spectra were collected for each matrix, providing a sufficient number of scans for a trustworthy comparison of the matrix performance. As the signal of $[M + Li]^+$ tended to last for a long time, the number of laser shots selected for the automatic measurement ensured sufficiently stable signals within the course of the measurement from a single spot. The average intensities and relative standard deviations (RSD) of $[M + Li]^+$ signals are given in Fig. 3. The RSD values were in the range of several dozen percent, which is expectable for this type of application. Several matrices provided higher average signals than LiDHB both for *n*-triacontane and stearyl behenate. Among them, LiVA gave the highest average signals (2.6× higher for ester and 8.6× higher for *n*-triacontane than LiDHB). At the same time, the RSD values of the LiVA signals were comparable with those of LiDHB or even better. Among other matrices, LiSA and LiSalA also performed quite well. The worst-performing matrices were LiBA and LiDMB, which provided only weak and poorly reproducible signals for the analytes tested. We carefully inspected mass spectra recorded in the tested matrices and searched for ions possibly formed by fragmentation or dehydrogenation of the lithium adducts. However, no such ions were found. Scanning electron microscopy (SEM) was used to learn whether or not the measured-signal RSD values reflect the sample-deposit homogeneity and morphology (see the supporting information, Figs. S10–S16). The SEM images revealed that most of the matrices formed deposits with a homogenous central part, both for stearyl behenate and *n*-triacontane. Depending on the matrix and sample preparation, crystals and features of various shapes were observed. The crystal diameters were usually in the

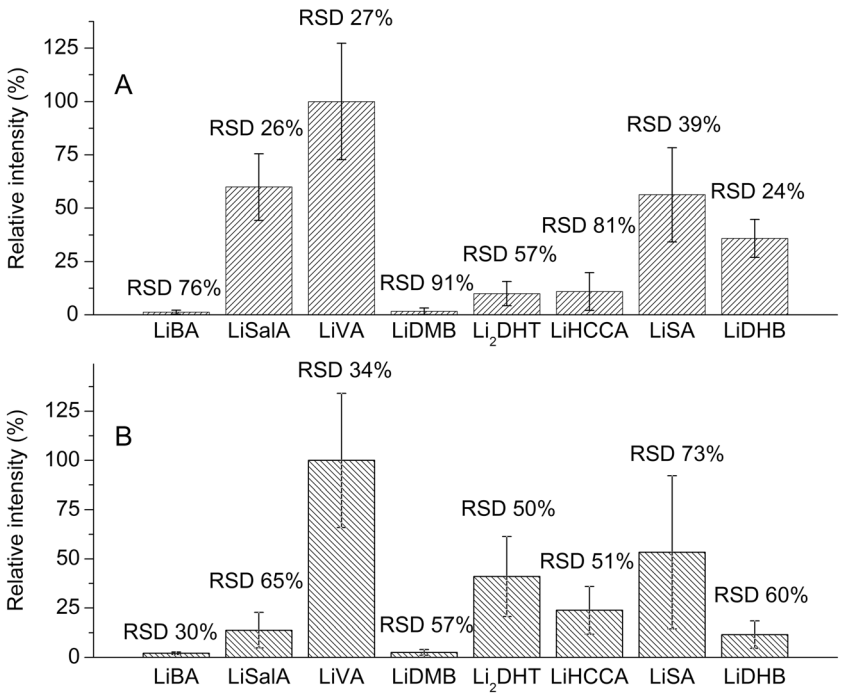

Figure 3. The average normalized intensities of $[M + Li]^+$ for stearyl behenate (A) and *n*-triacontane (B) in the investigated matrices. The error bars and the values above the columns represent standard deviations and relative standard deviations, respectively.

micrometer range with some exceptions (LiSalA and LiHCCA formed roughly ten times larger crystals in *n*-triacontane samples). Although samples with relatively less homogenous morphology (e.g. LiBA, LiDMB or LiHCCA) tended to provide less reproducible signals, SEM morphology was found to have rather low power to predict MALDI signal variability. A rough estimate of the detection limits for stearyl behenate and *n*-triacontane in the evaluated matrices was obtained from a calibration curve for signal-to-noise ratio 3 (supporting information, Table S5). Noise was measured as the standard deviation of the background signal in the regions free of analyte or matrix signals. The lowest detection limits were obtained using LiVA (48.3 pg for stearyl behenate, 2.8 ng for *n*-triacontane).

Our results indicate that modification of the functional groups strongly influenced practical usefulness of the MALDI matrices. Not surprisingly, the worst performing matrix was LiBA, which does not absorb UV radiation in the laser wavelength range. However, the UV absorption itself is not sufficient for good matrix. In case of LiDMB, which also failed to provide good quality $[M + Li]^+$ signal, the UV absorption profile (in solution) was very similar to that of LiSalA, one of the well-performing matrices. The solid-state spectrum of LiDMB showed a significant shift toward higher wavelengths, which increased absorption at 337 nm. By far the highest absorption coefficient at 337 nm was measured for LiHCCA, which showed only a moderate or weak ability to ionize the neutral lipids tested. Clearly, other factors besides ability to absorb UV radiation at the laser wavelength are highly important. One of them seems to be the ability to co-crystallize with the analyte and form homogenous deposits on the target, which can be related to solubility of the matrices in organic solvents. Indeed, the best-performing LiVA matrix exhibited high solubility both in CH_3OH and $CHCl_3$, which allowed us to prepare morphologically homogenous deposits in the $CH_3OH/CHCl_3$ system (see the supporting information, Fig. S12). Such samples provided high and relatively well-reproducible signals without a tendency to sweet-spot formation. The functional groups also influenced gas-phase lithium cation basicity of the matrix and thus possibly also its ability to transfer lithium cation to the analyte. Lithium can likely coordinate with one or two oxygens or other active sites on the matrix molecule. The theoretical calculations of the $DHBNa^+$ complex showed that the most stable structures are those, where sodium coordinates either with 2-hydroxyl and carboxylic oxygens, or where sodium is bound to both carboxylic oxygens and H-bond is formed between carboxylic hydrogen and the 2-hydroxyl oxygen.[59] Both compounds evaluated in this study as inappropriate matrices (LiBA and LiDMB) lacked hydroxyl substitution on the benzene ring, which possibly influenced their ability to bind lithium. Unfortunately, gas-phase lithium cation basicities are not available for the tested matrices, and thus no comparison with the results obtained here can be made.

In light of the results, LiVA was suggested as a suitable MALDI matrix for lithium cationization of neutral lipids with a superior performance over the already known LiDHB. LiVA was found to be compatible with the solvent systems used for long-chain neutral lipids and provided high and well-reproducible signals. Low laser-power settings sufficed for efficient ionization of the neutral lipids tested. In the case of LiDHB and MALDI of HCs, lithium adducts are usually not observed until several dozen laser 'pre-heating' shots are fired.[34] With LiVA, the activation period was found to be considerably shorter (using the optimum laser setting). The "pre-heating" period duration was not investigated further because the software did not allow us collecting time-resolved data. Among the other matrices tested, also LiSA and LiSalA provided good quality signals and were identified as suitable matrices for long-chain neutral lipids.

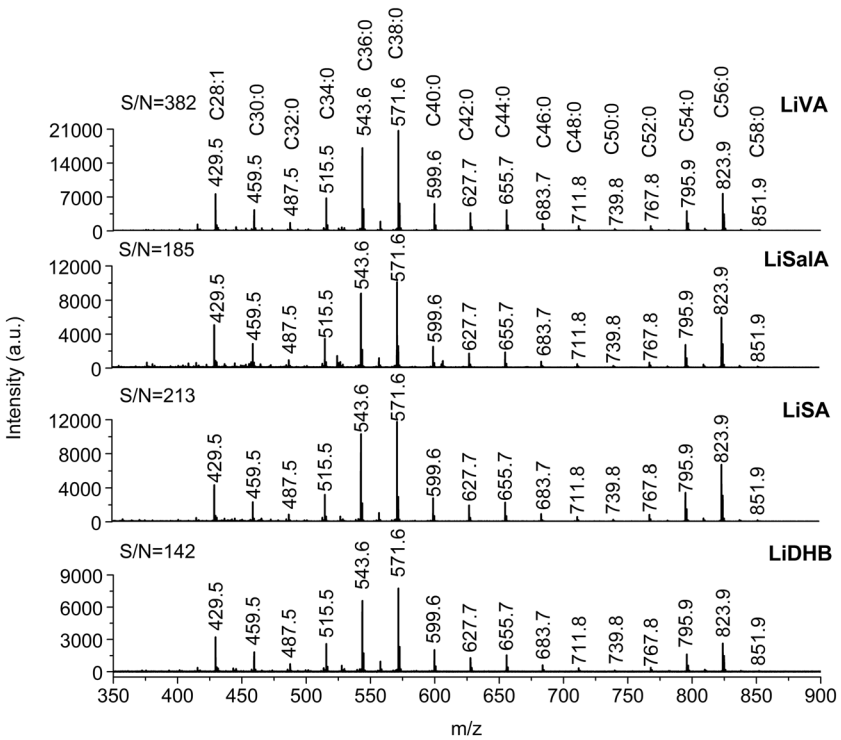

Figure 4. The MALDI spectra of wax esters isolated from *G. biloba* recorded in LiVA, LiSalA, LiSA and LiDHB matrices.

Journal of MASS SPECTROMETRY

Applications

The applicability of LiVA, LiSalA and LiSA for the analyses of WE or HC mixtures was tested using optimized conditions for sample preparation and MALDI-MS measurement as described above. The samples were deposited in triplicates at random positions on the target, and the spectra were recorded using an automatic measurement mode (10× for each sample position, 1000 shots).

Two samples of WEs were isolated from *G. biloba* leaves and virgin beeswax, and their MALDI spectra were recorded using LiVA, LiSalA, LiSA and LiDHB matrices (Figs. 4 and 5). For each sample, the spectra were well comparable among themselves in all matrices. The spectra showed $[M+Li]^+$ peaks of mostly saturated species with an even number of carbons (C28–C58 for *G. biloba*, C40–C50 for beeswax). They were also consistent with our previously published data[37]; the minor differences were

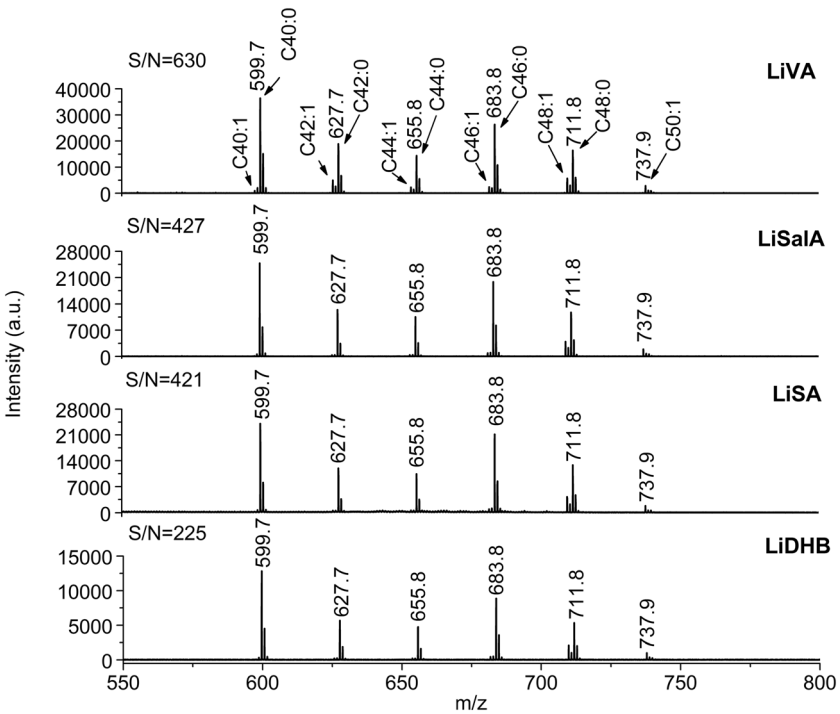

Figure 5. The MALDI spectra of wax esters isolated from beeswax recorded in LiVA, LiSalA, LiSA and LiDHB matrices.

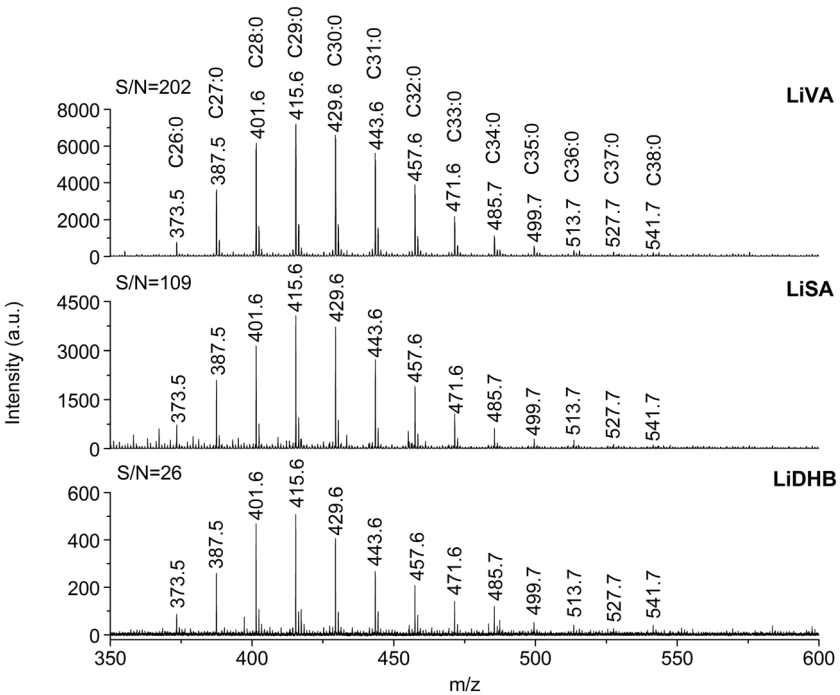

Figure 6. The MALDI spectra of HCs isolated from Parafilm® M recorded in LiVA, LiSA and LiDHB matrices.

assigned to the variability of the biological material used for the isolation of WEs. The minor signals at two mass unit smaller *m/z* values represented singly unsaturated WEs in the sample. Their presence was confirmed by GC/MS analysis of the sample (data not shown). When the spectra intensities were compared, the newly synthesized matrices provided higher signals of $[M+Li]^+$ than LiDHB. The most significant increase of the signal was observed for LiVA (2.7× for *G. biloba*, 2.8× for beeswax). Clearly, LiVA, LiSalA and LiSA provided a better performance for the MALDI analysis of WEs than LiDHB.

A relatively simple test mixture of HCs was isolated from the laboratory sealing film Parafilm® M. GC/MS analysis revealed that a chloroform extract of Parafilm® M contained straight-chain HCs C20–C50 with a small amount of methyl-branched (mostly *iso* and *anteiso*) and unsaturated HCs (supporting information, Fig. S17). When analyzed by MALDI-MS, $[M+Li]^+$ signals consistent with saturated HCs (C26–C38) were observed (Fig. 6). Like in the case of WEs, the spectrum appearance was almost alike for the matrices tested (LiVA, LiSA, LiDHB), the main difference being the signal intensities. The highest gain of the signal was observed for LiVA (7.7× higher than for LiDHB). The cuticular HCs of *N. bullata* represent a substantially more complex mixture of HCs. They are known to be composed of straight-chain, methyl-branched, multiply-methyl branched and unsaturated (up to four double bonds) HCs with up to 50 carbon atoms.[36,39,60,61] Like in the previous case, the tested matrices provided $[M+Li]^+$ ions with the signal intensities for LiVA and LiSA significantly higher than for LiDHB (signal for LiVA 9.8× higher than for LiDHB; Fig. 7). Although the signals appeared at the same *m/z* values, significant differences in the relative peak abundances were found. We hypothesized that these differences were connected with the reproducibility of the measurement. To confirm this hypothesis, the spectra were transformed to peak lists and investigated using PCA. Figure 8 depicts the graphical representation of the factor scores of the first two factors based on 13 measurements for each matrix. Obviously, the distributions of the factor scores corresponding to LiDHB and LiSA matrices are dramatically more heterogeneous than the homogenous cluster of LiVA measurements, suggesting a better reproducibility of LiVA spectra with the minimum outlying observations. The results of the PCA are in agreement with the reproducibility data obtained for the standard of *n*-triacontane, where the RSD values for LiSA and LiDHB were roughly twice as high as those recorded for LiVA. These results further confirm the superior performance of LiVA.

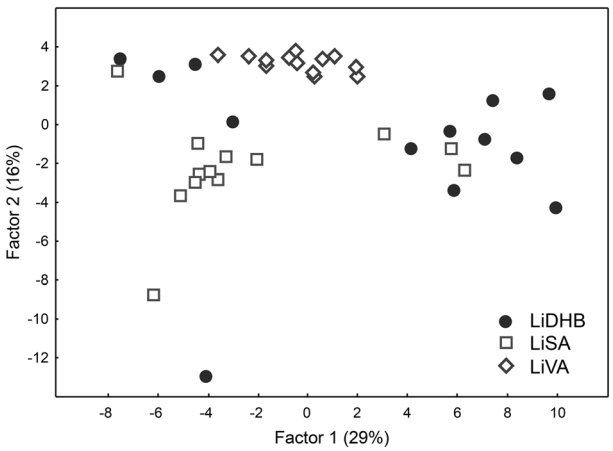

Figure 8. The factor scores of the first two components of the principal component analysis calculated from the relative intensities of $[M+Li]^+$ adducts of cuticular HCs isolated from *N. bullata* and recorded in LiVA, LiSA and LiDHB matrices.

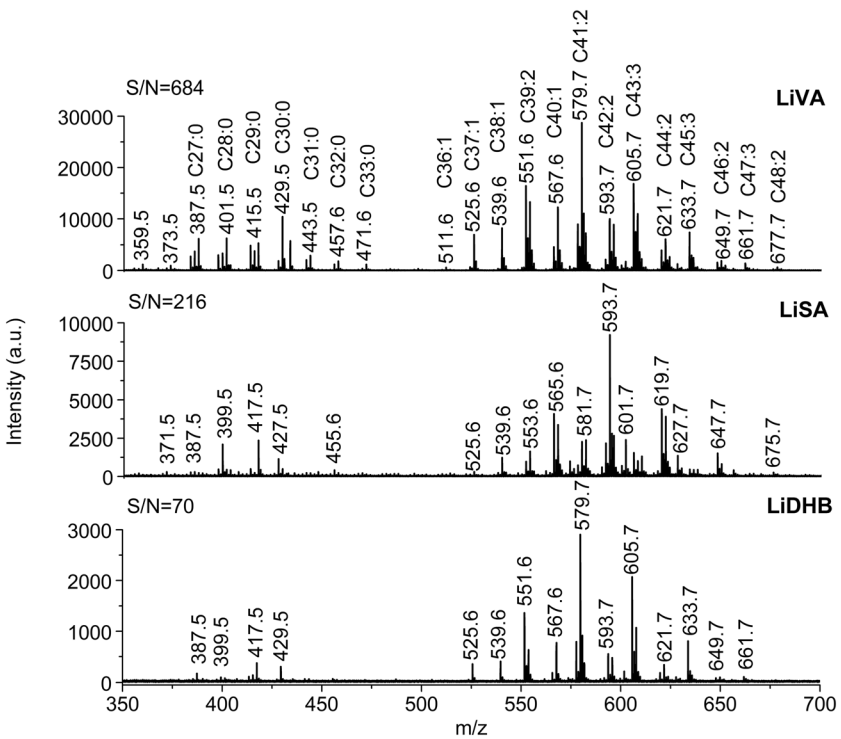

Figure 7. The MALDI spectra of cuticular HCs isolated from *N. bullata* recorded in LiVA, LiSA and LiDHB matrices.

Journal of MASS SPECTROMETRY

Moreover, only LiVA allowed for the detection of saturated shorter-chain HCs in the 350–450 *m/z* range (e.g. *m/z* 387.5, *m/z* 401.6, *m/z* 415.6 and *m/z* 443.6), which were shown previously[36] to be constituents of *N. bullata* cuticular HCs. Short-chain HCs were likely well embedded in LiVA crystals, which prevented them to volatilize in vacuum.

Conclusions

Systematic variation of the functional groups on the core structure can be a successful approach in the matrix engineering.[62] Here, three new UV MALDI matrices based on the lithium salts of aromatic acids with a better performance than the already known LiDHB matrix were identified. Lithium vanillate, lithium sinapate and lithium salicylate allowed for a sensitive detection of the standards as well as analytes in the complex mixtures of long-chain HCs and WEs. Among them, lithium vanillate performed the best, providing the strongest signals and the most reproducible spectra. The exceptional properties of lithium vanillate were explained by adequate absorptions of UV radiation and the enhanced solubility of the matrix in the organic solvents used for the preparation of the samples of a very low polarity. In addition, the structure of lithium vanillate may support efficient transfer of lithium cation to the analyte in the gas phase. Lithium vanillate tended to form homogenous deposits as evidenced also from the SEM images of the samples. We concluded that it might be a suitable candidate for MSI applications. We also shortly tested lithium vanillate and LiDHB matrices with Bruker's UltrafleXtreme MALDI-TOF/TOF equipped with 1-kHz smartbeam II laser at 355 nm. The matrices provided abundant signals of $[M+Li]^+$ both for stearyl behenate and *n*-triacontane indicating that the lithium-based matrices might also be useful for MALDI with 355-nm lasers.

Acknowledgements

This work was supported by the Czech Science Foundation (GACR, Project No. 203/09/0139), the Academy of Sciences of the Czech Republic (RVO: 61388963) and Charles University in Prague (Project SVV 260084). The authors are indebted to Kamil Lang, Petr Rychlovský, and Stanislava Matějková for their help with measurements and fruitful discussions.

References

[1] R. J. Hamilton (Ed.). Waxes: Chemistry, Molecular Biology and Functions, Oily Press: Dundee, **1995**.
[2] L. Kunst, A. L. Samuels. Biosynthesis and secretion of plant cuticular wax. *Prog. Lipid Res.* **2003**, *42*, 51.
[3] R. F. Lee, W. Hagen, G. Kattner. Lipid storage in marine zooplankton. *Mar. Ecol. Prog. Ser.* **2006**, *307*, 273.
[4] K. R. Smith, D. M. Thiboutot. Sebaceous gland lipids: friend or foe? *J. Lipid Res.* **2008**, *49*, 271.
[5] G. J. Blomquist, A. Bagnères. Insect Hydrocarbons. Biology, Biochemistry and Chemical Ecology, Cambridge University Press: New York, **2010**.
[6] S. D. Killops, R. M. K. Carlson, K. E. Peter. High-temperature GC evidence for the early formation of C40+ n-alkanes in coals. *Org. Geochem.* **2000**, *31*, 589.
[7] P. A. Sutton, S. J. Rowland. High temperature gas chromatography–time-of-flight-mass spectrometry (HTGC–ToF-MS) for high-boiling compounds. *J. Chromatogr. A* **2012**, *1243*, 69.
[8] P. A. Sutton, M. J. Wilde, S. J. Martin, J. Cvačka, V. Vrkoslav, S. J. Rowland. Studies of long chain lipids in insects by high temperature gas chromatography and high temperature gas chromatography–mass spectrometry. *J. Chromatogr. A* **2013**, *1297*, 236.
[9] A. Dagan, A. Amirav. Electron-impact mass-spectrometry of alkanes in supersonic molecular-beams. *J. Am. Soc. Mass Spectrom.* **1995**, *6*, 120.
[10] A. B. Fialkov, U. Steiner, L. Jones, A. Amirav. A new type of GC-MS with advanced capabilities. *Int. J. Mass Spectrom.* **2006**, *251*, 58.
[11] M. Holčapek, H. Velínská, M. Lísa, P. Česla. Orthogonality of silver-ion and non-aqueous reversed-phase HPLC/MS in the analysis of complex natural mixtures of triacylglycerols. *J. Sep. Sci.* **2009**, *32*, 3672.
[12] V. Vrkoslav, K. Urbanová, J. Cvačka. Analysis of wax ester molecular species by high-performance liquid chromatography/atmospheric pressure chemical ionisation mass spectrometry. *J. Chromatogr. A* **2010**, *1217*, 4184.
[13] J. M. Rocha, P. J. Kalo, V. Ollilainen, F. X. Malcata. Separation and identification of neutral cereal lipids by normal phase high-performance liquid chromatography, using evaporative light-scattering and electrospray mass spectrometry for detection. *J. Chromatogr. A* **2010**, *1217*, 3013.
[14] M. Lisa, K. Netusilova, L. Franek, H. Dvořáková, V. Vrkoslav, M. Holčapek. Characterization of fatty acid and triacylglycerol composition in animal fats using silver-ion and non-aqueous reversed-phase high-performance liquid chromatography/mass spectrometry and gas chromatography/flame ionization detection. *J. Chromatogr. A* **2011**, *1218*, 7499.
[15] S. M. Momchilova, B. M. Nikolova-Damyanova. Advances in silver ion chromatography for the analysis of fatty acids and triacylglycerols – 2001 to 2011. *Anal. Sci.* **2012**, *28*, 837.
[16] V. Vrkoslav, K. Urbanová, M. Háková, J. Cvačka. Analysis of wax esters by silver-ion high-performance liquid chromatography-tandem mass spectrometry. *J. Chromatogr. A* **2013**, *1302*, 105.
[17] V. Vrkoslav, M. Háková, K. Pecková, K. Urbanová, J. Cvačka. Localization of double bonds in wax esters by high-performance liquid chromatography/atmospheric pressure chemical ionization mass spectrometry utilizing the fragmentation of acetonitrile-related adducts. *Anal. Chem.* **2011**, *83*, 2978.
[18] J. Gao, B. C. Owen, D. J. Borton, Z. Jin, H. I. Kenttämaa. HPLC/APCI mass spectrometry of saturated and unsaturated hydrocarbons by using hydrocarbon solvents as the APCI reagent and HPLC mobile phase. *J. Am. Soc. Mass Spectrom.* **2012**, *23*, 816.
[19] M. Lísa, M. Holčapek. Characterization of triacylglycerol enantiomers using chiral HPLC/APCI-MS and synthesis of enantiomeric triacylglycerols. *Anal. Chem.* **2013**, *85*, 1852.
[20] A. Medvedovici, K. Lazou, A. d'Oosterlinck, Y. Zhao, P. Sandra. Analysis of jojoba oil by LC-coordination ion spray-MS (LC-CIS-MS). *J. Sep. Sci.* **2002**, *25*, 173.
[21] S. Santos, L. Schreiber, J. Graça. Cuticular waxes from ivy leaves (*Hedera helix* L.): Analysis of high-molecular-weight esters. *Phytochem. Anal.* **2007**, *18*, 60.
[22] P. M. Hutchins, R. M. Barkley, R. C. Murphy. Separation of cellular nonpolar neutral lipids by normal-phase chromatography and analysis by electrospray ionization mass spectrometry. *J. Lipid Res.* **2008**, *49*, 804.
[23] S. M. Lam, L. Tong, B. Reux, M. J. Lear, M. R. Wenk, G. Shui. Rapid and sensitive profiling of tear wax ester species using high performance liquid chromatography coupled with tandem mass spectrometry. *J. Chromatogr. A* **2013**, *1308*, 166.
[24] J. H. Gross, K. Vekey, A. Dallos. Field desorption mass spectrometry of large multiply branched saturated hydrocarbons. *J. Mass Spectrom.* **2001**, *36*, 522.
[25] T. M. Schaub, C. L. Hendrickson, J. P. Quinn, R. P. Rodgers, A. G. Marshall. Instrumentation and method for ultrahigh resolution field desorption ionization Fourier transform ion cyclotron resonance mass spectrometry of nonpolar species. *Anal. Chem.* **2005**, *77*, 1317.
[26] C. Wu, K. Qian, M. Nefliu, R. G. Cooks. Ambient analysis of saturated hydrocarbons using discharge-induced oxidation in desorption electrospray ionization. *J. Am. Soc. Mass Spectrom.* **2010**, *21*, 261.
[27] A. U. Jackson, T. Shum, E. Sokol, A. Dill, R. G. Cooks. Enhanced detection of olefins using ambient ionization mass spectrometry: Ag^+ adducts of biologically relevant alkenes. *Anal. Bioanal. Chem.* **2011**, *399*, 367.
[28] N. M. Suni, H. Aalto, T. J. Kauppila, T. Kotiaho, R. Kostiainen. Analysis of lipids with desorption atmospheric pressure photoionization-mass spectrometry (DAPPI-MS) and desorption electrospray ionization-mass spectrometry (DESI-MS). *J. Mass Spectrom.* **2012**, *47*, 611.
[29] J. K. Pruns, C. Rapp, U. Hintze, K. P. Wittern, W. A. Konig. Characterization of paraffin oils and petrolatum using LDI-TOF MS and principle component analysis. *Eur. J. Lipid Sci. Technol.* **2003**, *105*, 275.
[30] H. P. Nguyen, I. P. Ortiz, C. Temiyasathit, S. B. Kim, K. A. Schug. Laser desorption/ionization mass spectrometry fingerprinting of complex

hydrocarbon mixtures: application to crude oils using data mining techniques. *Rapid Commun. Mass Spectrom.* **2008**, *22*, 2220.
[31] J. Y. Yew, K. Dreisewerd, H. Luftmann, J. Müthin, G. Pohlentz, E. A. Kravitz. A new male sex pheromone and novel cuticular cues for chemical communication in *Drosophila*. *Curr. Biol.* **2009**, *19*, 1245.
[32] J. Y. Yew, J. Soltwisch, A. Pirkl, K. Dreisewerd. Direct laser desorption ionization of endogenous and exogenous compounds from insect cuticles: Practical and methodologic aspects. *J. Am. Soc. Mass Spectrom.* **2011**, *22*, 1273.
[33] P. O. Danis, D. E. Karr, Y. Xiong, K. G. Owens. Methods for the analysis of hydrocarbon polymers by matrix-assisted laser desorption/ionization time-of-flight mass spectrometry. *Rapid Commun. Mass Spectrom.* **1996**, *10*, 862.
[34] J. Cvačka, A. Svatoš. Matrix-assisted laser desorption/ionization analysis of lipids and high molecular weight hydrocarbons with lithium 2,5-dihydroxybenzoate matrix. *Rapid Commun. Mass Spectrom.* **2003**, *17*, 2203.
[35] A. J. Jaber, C. L. Wilkins. Hydrocarbon polymer analysis by external MALDI Fourier transform and reflectron time of flight mass spectrometry. *J. Am. Soc. Mass Spectrom.* **2005**, *16*, 2009.
[36] J. Cvačka, P. Jiroš, J. Šobotník, R. Hanus, A. Svatoš. Analysis of insect cuticular hydrocarbons using matrix-assisted laser desorption/ionization mass spectrometry. *J. Chem. Ecol.* **2006**, *32*, 409.
[37] V. Vrkoslav, R. Míková, J. Cvačka. Characterization of natural wax esters by MALDI-TOF mass spectrometry. *J. Mass Spectrom.* **2009**, *44*, 101.
[38] B. Fuchs, R. Süβ, J. Schiller. An update of MALDI-TOF mass spectrometry in lipid research. *Prog. Lipid Res.* **2010**, *49*, 450.
[39] V. Vrkoslav, A. Muck, J. Cvačka, A. Svatoš. MALDI imaging of neutral cuticular lipids in insects and plants. *J. Am. Soc. Mass Spectrom.* **2010**, *21*, 220.
[40] A. Svatoš. Mass spectrometric imaging of small molecules. *Trends Biotechnol.* **2010**, *28*, 425.
[41] K. A. Zemski Berry, J. A. Hankin, R. M. Barkley, J. M. Spraggins, R. M. Caprioli, R. C. Murphy. MALDI imaging of lipid biochemistry in tissues by mass spectrometry. *Chem. Rev.* **2011**, *111*, 6491.
[42] D. Gode, D. A. Volmer. Lipid imaging by mass spectrometry – a review. *Analyst* **2013**, *138*, 1289.
[43] G. Kuhn, S. Weidner, U. Just, G. Hohner. Characterization of technical waxes – Comparison of chromatographic techniques and matrix assisted laser-desorption/ionization mass spectrometry. *J. Chromatogr. A* **1996**, *732*, 111.
[44] T. K. Dutta, S. Harayama. Time-of-flight mass spectrometric analysis of high-molecular-weight alkanes in crude oil by silver nitrate chemical ionization after laser desorption. *Anal. Chem.* **2001**, *73*, 864.
[45] J. K. Pruns, J. P. Vietzke, M. Strassner, C. Rapp, U. Hintze, W. A. Konig. Characterization of low molecular weight hydrocarbon oligomers by laser desorption/ionization time-of-flight mass spectrometry using a solvent-free sample preparation method. *Rapid Commun. Mass Spectrom.* **2002**, *16*, 208.
[46] E. Suarez, H. P. Nguyen, I. P. Ortiz, K. J. Lee, S. B. Kim, J. Krzywinski, K. A. Schug. Matrix-assisted laser desorption/ionization-mass spectrometry of cuticular lipid profiles can differentiate sex, age, and mating status of *Anopheles gambiae* mosquitoes. *Anal. Chim. Acta* **2011**, *706*, 157.
[47] E. Lorente, C. Berrueco, A. A. Herod, M. Millan, R. Kandiyoti. The detection of high-mass aliphatics in petroleum by matrix-assisted laser desorption/ionisation mass spectrometry. *Rapid Commun. Mass Spectrom.* **2012**, *26*, 1581.
[48] S. F. Macha, P. A. Limbach, S. D. Hanton, K. G. Owens. Silver cluster interferences in matrix-assisted laser desorption/ionization (MALDI) mass spectrometry of nonpolar polymers. *J. Am. Soc. Mass Spectrom.* **2001**, *12*, 732.
[49] J. Zhang, R. Zenobi. Matrix-dependent cationization in MALDI mass spectrometry. *J. Mass Spectrom.* **2004**, *39*, 808.
[50] J. Jover, R. Bosque, J. Sales. Determination of lithium cation basicity from molecular structure. *J. Chem. Inf. Comput. Sci.* **2004**, *44*, 1727.
[51] T. H. James, J. M. Snell, A. Weissberger. Oxidation Processes. XII. The Autoxidation of Hydroquinone and of the Mono-, Di- and Trimethylhydroquinones. *J. Am. Chem. Soc.* **1938**, *60*, 2084.
[52] J. Torrent, V. Barron. Diffuse reflectance spectroscopy. In Methods of Soil Analysis, A. L. Ulery, L. R. Drees (Eds). Soil Science Society of America: Madison, **2008**, 367–387.
[53] P. Kubelka, F. Munk. Ein Beitrag zur Optik der Farbanstriche. *Z. Tech. Phys.* **1931**, *12*, 593.
[54] V. Horneffer, K. Dreisewerd, H.-C. Ludemann, F. Hillenkamp, M. Lage, K. Strupat. Is the incorporation of analytes into matrix crystals a prerequisite for matrix-assisted laser desorption/ionization mass spectrometry? A study of five positional isomers of dihydroxybenzoic acid. *Int. J. Mass Spectrom.* **1999**, *185/186/187*, 859.
[55] J. Schiller, J. Arnhold, S. Bernard, M. Müller, S. Reich, K. Arnold. Lipid analysis by matrix-assisted laser desorption and ionization mass spectrometry: A methodological approach. *Anal. Biochem.* **1999**, *267*, 46.
[56] M. J. Kang, A. Tholey, E. Heinzle. Quantitation of low molecular mass substrates and products of enzyme catalyzed reactions using matrix-assisted laser desorption/ionization time-of-flight mass spectrometry. *Rapid Commun. Mass Spectrom.* **2000**, *14*, 1972.
[57] S. Trimpin, A. Rouhanipour, R. Az, H. J. Räder, K. Müllen. New aspects in matrix-assisted laser desorption/ionization time-of-flight mass spectrometry: a universal solvent-free sample preparation. *Rapid Commun. Mass Spectrom.* **2001**, *15*, 1364.
[58] A. Tholey, E. Heinzle. Ionic (liquid) matrices for matrix-assisted laser desorption/ionization mass spectrometry-applications and perspectives. *Anal. Bioanal. Chem.* **2006**, *386*, 24.
[59] J. Zhang, T.-K. Ha, R. Knochenmuss, R. Zenobi. Theoretical Calculation of Gas-Phase of Common MALDI Matrices. *J. Phys. Chem. A* **2002**, *106*, 6610.
[60] L. L. Jackson, M. T. Armold, F. E. Regnier. Cuticular lipids of adult fleshflies, *Sarcophaga bullata*. *Insect Biochem.* **1974**, *4*, 369.
[61] M. T. Armold, F. E. Regnier. A developmental study of the cuticular hydrocarbons of *Sarcophaga bullata*. *J. Insect Physiol.* **1975**, *21*, 1827.
[62] T. W. Jaskolla, W. D. Lehmann, M. Karas. 4-Chloro-alpha-cyanocinnamic acid is an advanced, rationally designed MALDI matrix. *Proc. Natl. Acad. Sci. U. S. A.* **2008**, *105*, 12200.

Supporting information

Additional supporting information may be found in the online version of this article at the publisher's web-site.